AGU PUBLICATIONS

Geophysical Research Letters

RESEARCH LETTER
10.1002/2015GL067298

Key Points:
- Viscous flow is not important for presently observed impact craters on the NPLD of Mars
- Steep scarps at the NPLD margins experience flow on the order of tens to hundreds of cm/yr
- We propose a theory for NPLD scarp evolution relating flow to avalanches and block falls

Supporting Information:
- Supporting Information S1
- Figure S1

Correspondence to:
M. M. Sori,
sori@lpl.arizona.edu

Citation:
Sori, M. M., S. Byrne, C. W. Hamilton, and M. E. Landis (2016), Viscous flow rates of icy topography on the north polar layered deposits of Mars, *Geophys. Res. Lett.*, *43*, doi:10.1002/2015GL067298.

Received 4 DEC 2015
Accepted 28 DEC 2015
Accepted article online 30 DEC 2015

Viscous flow rates of icy topography on the north polar layered deposits of Mars

Michael M. Sori[1], Shane Byrne[1], Christopher W. Hamilton[1], and Margaret E. Landis[1]

[1]Lunar and Planetary Laboratory, University of Arizona, Tucson, Arizona, USA

Abstract We investigate the importance of viscous flow in shaping topography at the north polar layered deposits (NPLD) of Mars by using finite element modeling to calculate the distribution of stresses and flow velocities. Present-day impact craters on the NPLD are too small and cold for viscous relaxation to have been an important mechanism in controlling their current dimensions; this effect may be ignored when analyzing crater size-frequency distributions. Scarps at the NPLD margins, where avalanches of dust and carbon dioxide frost occur, are sufficiently steep, high, and warm to experience significant viscous flow. We find flow velocities at the base of these steep scarps on the order of tens to hundreds of cm/yr, which are fast enough to significantly affect their slope over kiloyear timescales. Alternatively, the scarps could be close to steady state in which observed block falls provide a competing effect to viscous flow.

1. Introduction

Topography may be significantly altered by viscous flow over sufficiently long timescales. Viscosities of silicate rocks are generally too high for viscous relaxation to be an important modifier of rocky topography on terrestrial planetary surfaces [e.g., *Melosh*, 2011], but the viscosity of water ice is much lower. Viscous flow of terrestrial glaciers has been well documented, with observed flow velocities typically on the order of one to tens of m/yr [e.g., *Cuffey and Paterson*, 2010]. The rates of similar processes on other planets are less certain. There is topography on icy moons that was likely modified in part by viscous flow, such as lobate features on Europa [*Miyamoto et al*., 2005] and shallow craters on Enceladus [*Bland et al*., 2012]. However, predictions of smooth and geologically young surfaces due to complete viscous relaxation of impact craters coupled with contradicting observations of heavily cratered surfaces are a recurring theme in studies of the outer solar system (e.g., Ganymede [*Thomas and Schubert*, 1988; *Dombard and McKinnon*, 2000]). Thus, while viscous relaxation at a global scale [e.g., *Nimmo*, 2005] is likely important in planetary histories, the efficiency of viscous flow in shaping topography at regional or local scales is uncertain.

Viscous flow was first proposed as important in shaping Martian landforms based on Mariner 9 spacecraft imagery of midlatitude regions [*Squyres*, 1978], an idea confirmed by subsequent observations and modeling [e.g., *Milliken et al*., 2003]. Here we focus on the poles, where there are kilometers thick layered sedimentary deposits first observed by Mariner 9 [*Murray et al*., 1972] composed of dusty ice. Water ice is by far the largest constituent by mass or volume of these north and south polar layered deposits (NPLD and SPLD, respectively); CO_2 and clathrate hydrate have been shown to be negligible in the NPLD from studies of thermal properties [*Mellon*, 1996] and bulk strength [*Nye et al*., 2000], although soundings by the Mars Reconnaissance Orbiter Shallow Radar (SHARAD) instrument reveal ~10^4 km^3 of CO_2 ice overlying parts of the SPLD (~1% of the SPLD by volume) [*Phillips et al*., 2011]. Dust volume is no greater than 5% in the NPLD [*Picardi et al*., 2005; *Grima et al*., 2009] and 10% in the SPLD [*Plaut et al*., 2007] on the basis of SHARAD data, while gravity analyses suggest higher values of ~15% in the SPLD [*Zuber et al*., 2007; *Wieczorek*, 2008]. Snow and firn are common in the upper decameters of terrestrial ice sheets and have important effects on flow [e.g., *Zwinger et al*., 2007] but are not expected here because under recent climatic conditions water ice forms by direct deposition, not precipitation. Low porosities are predicted [*Arthern et al*., 2000] and supported by observations [*Langevin et al*., 2005].

Whether the NPLD flow as a whole structure has been debated [*Byrne*, 2009]. Mechanical models have shown that the shape of the whole PLD could be consistent with flow over large regions, with the flow magnitude dependent upon the assumed heat flux [*Nye*, 2000]. However, topographic measurements suggest that slopes at the margins may generally be too steep to be primarily controlled by viscous flow. Flow features could be preserved from a higher-obliquity era [*Zuber et al*., 1998; *Greve*, 2000]. Analysis of the surface of

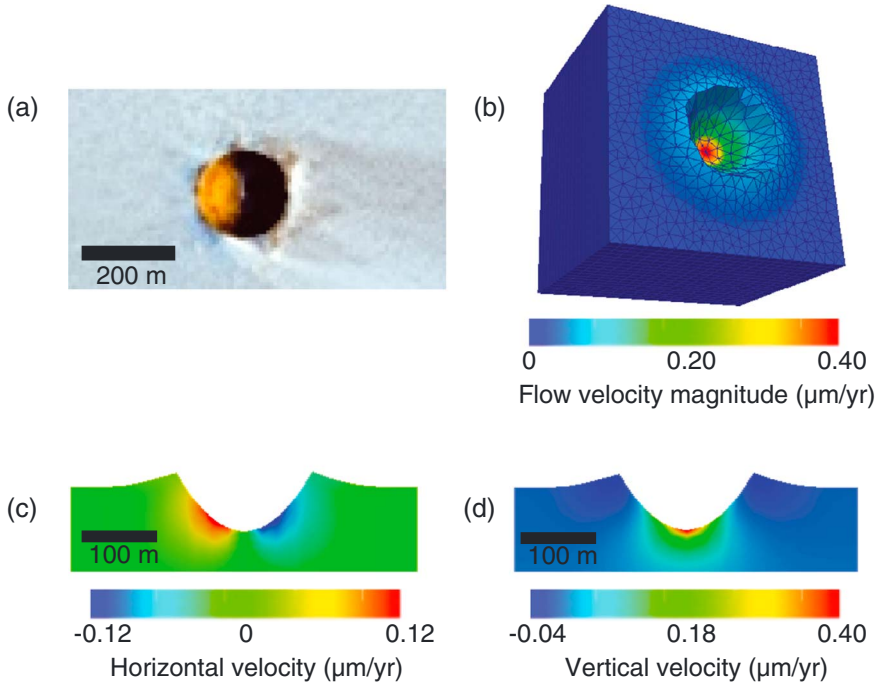

Figure 1. Results for a 200 m diameter impact crater at 170 K in the NPLD, such as the one observed in (a) HiRISE image PSP_009773_2675. (b) Total, (c) horizontal, and (d) vertical flow velocities do not exceed μm/yr (positive directions are up/right). See text for model parameters. Nodes/elements plotted on Figure 1b.

Gemina Lingula (an NPLD lobe) showed that its shape and slopes are consistent with a flowing ice mass [*Winebrenner et al.*, 2008], but SHARAD data revealed that the internal stratigraphy is inconsistent with an ice sheet that has undergone significant flow [*Karlsson et al.*, 2011].

While the PLD are generally smooth with gentle slopes [*Zuber et al.*, 1998], they both contain icy topographic features, including troughs, craters, and scarps. Even studies that rule out flow as important in shaping the PLD as a whole [e.g., *Karlsson et al.*, 2011] allow for flow of topography locally, and indeed some of these features are expected to experience enhanced flow relative to smoother parts of the deposits [*Hvidberg*, 2003]. These features include spiraling troughs that cut into the PLD, exposing them. Troughs likely form as a result of positive feedback between slope and ablation [e.g., *Howard*, 1978] and migrate poleward through the PLD by wind transport as cyclic steps [*Smith et al.*, 2013]. However, a study that used the finite element method (FEM) to model viscous creep found that flow of subsurface ice may be the dominant mechanism in controlling NPLD trough morphology [*Pathare and Paige*, 2005].

Pathare et al. [2005] applied FEM simulations to the SPLD, focusing on impact craters. Impact craters on the PLDs are sparse relative to ancient rocky Martian terrain but exist in the NPLD [*Banks et al.*, 2010] and SPLD [*Koutnik et al.*, 2002]. *Pathare et al.* [2005] found that SPLD craters undergo extensive relaxation during their lifetime, and their distribution and depths are more likely to be controlled by viscous flow than by any other single modification mechanism. However, a complex history involving a combination of depositional and erosional processes could not be ruled out. Their study concluded that the SPLD were older (hundreds of megayears) than previously assumed and must be mostly water ice based on rheological constraints.

The NPLD surface is particularly young, with fewer and smaller craters than the SPLD. Searches of MRO Context Camera and High Resolution Imaging Science Experiment (HiRISE) [*McEwen et al.*, 2007] imagery have yielded 38 observed impact craters on the NPLD with diameter larger than 44 m (e.g., Figure 1a) [*Banks et al.*, 2010; *Landis et al.*, 2015]. When combined with a newly estimated production function of small impact craters on Mars based on HiRISE imagery [*Daubar et al.*, 2013], this yields a surface age on the order of kiloyears [*Landis et al.*, 2015]. The young surface age, smaller crater size, and lower dust content raises the question as to whether viscous relaxation of craters is as important on the NPLD as it is on the SPLD [*Pathare et al.*, 2005].

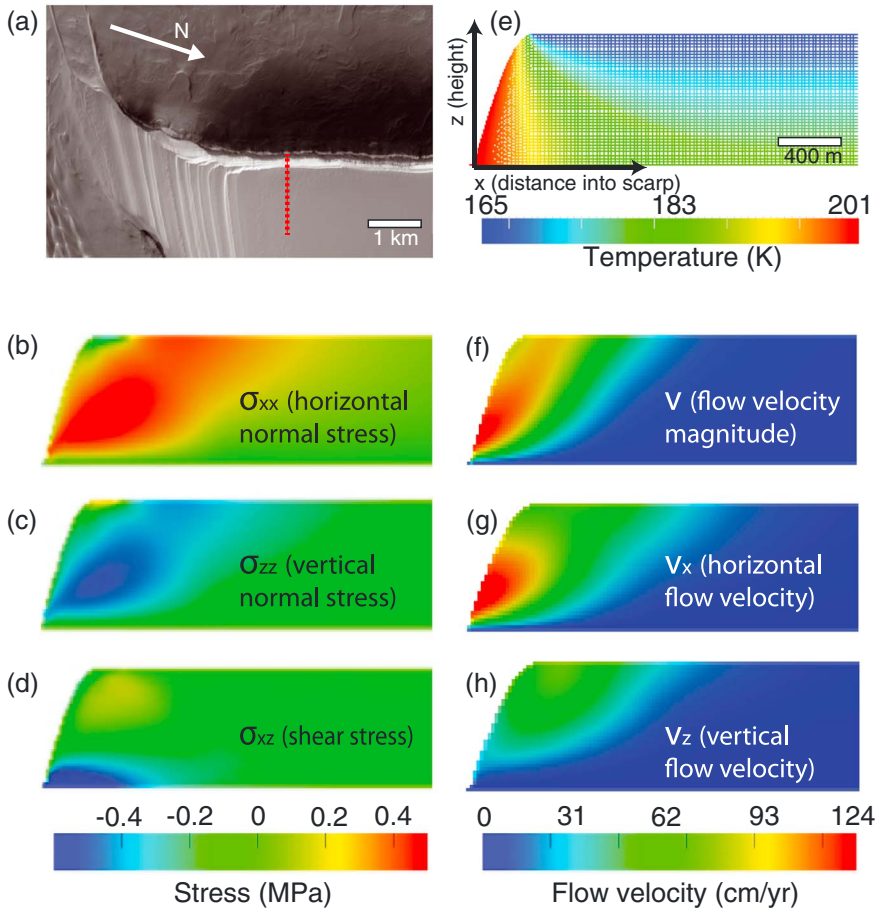

Figure 2. Results for a scarp 800 m high and 400 m wide, with a maximum slope of ~70°. (a) One scarp at the NPLD margin is shown, HiRISE image PSP_007140_2640; red dashed line traces an example 2-D profile as seen in the other panels. (b–d) Components of the deviatoric stresses. (e) The distribution of ice temperature. (f–h) Flow velocities. Positive directions are left/down. See text for model parameters. Nodes/elements are plotted on Figure 2e.

Steep scarps of ice have been observed at the fringes of the NPLD (e.g., Figure 2a). The scarps have a maximum slope of 60°–70° over a baseline of ~300 m, with sections as thick as ~100 m approaching 90° slopes [*Russell et al.*, 2008]. These slopes are far steeper than troughs in the NPLD interior, which are typically <15° [*Ivanov and Muhleman*, 2000]. The scarps experience relatively warm annual average temperatures due to their locations at the margins and steep equatorward facing slopes. The bases of these scarps are in contact with the basal unit (BU), a unit with gentler-sloping exposures of alternating bright and erosionally resistant layers with sandy and weakly consolidated layers that underlay the NPLD [*Herkenhoff et al.*, 2007]. The importance of gravity-driven viscous flow increases with slope, thickness, and temperature; thus, the morphology and location of the scarps make them a prime candidate for viscous relaxation.

Monitoring by HiRISE has revealed seasonally active avalanches occurring on these scarps [*Russell et al.*, 2008]. Such avalanches are likely primarily composed of dust and CO_2 frost sourced from the seasonal CO_2 ice cap. Although evidence exists that the events may contribute to mass wasting in the BU layer by triggering block fall of previously fractured BU bright layers [*Herkenhoff et al.*, 2007], there is no indication that avalanches directly transport mass from the NPLD. However, avalanches do redistribute volatiles and dust and could have indirect effects on scarp evolution. We suggest that these events may have important effects on potential viscous flow, as scouring of dust from scarp faces can alter their thermal properties (see section 3).

In this paper, we use a FEM (Elmer/Ice) to model viscous flow of topographic features in the NPLD. This follows the technique of previous work that assessed the importance of flow in NPLD troughs [*Pathare and Paige*, 2005], in SPLD craters [*Pathare et al.*, 2005], and along a line of longitude for the entire NPLD [*Hvidberg*, 2003]. Here we model NPLD craters [*Banks et al.*, 2010] and steep NPLD scarps that experience

avalanches [*Russell et al.*, 2008]. We quantify stresses, temperatures, and flow velocities to learn about timescales over which the topography flows, constraints on the age of the features, and the importance of viscous flow at the Martian poles.

2. Methods

We use the FEM code Elmer/Ice [*Gagliardini et al.*, 2013], which was developed specifically for glaciological and ice dynamics problems. The code solves the Navier-Stokes equations for the conservation of linear momentum and mass over a volume of ice. For simulations that are not isothermal, the code solves the heat equation, and the simulation is thermomechanically coupled. Elmer/Ice was largely developed for problems in terrestrial glaciology, but we adapt the model for Mars by changing the rheology laws and other important parameters.

Rheology is important to reconsider because the relative importance of various types of ice deformation may be different compared to the case of glaciers on Earth. Studies of terrestrial ice sheets often use the non-Newtonian Glen-Nye flow law [*Glen*, 1955], in which strain rate is proportional to stress raised to an exponent n. Here we instead separately calculate strain rate due to different modes of deformation: dislocation creep, grain boundary sliding (GBS), and basal slip. Each strain rate has the form

$$\dot{\varepsilon} = Ae^{-2n\phi}e^{-\frac{Q}{RT}}\tau^n d^m \tag{1}$$

where A is the material parameter, R is the gas constant, Q is activation energy, T is temperature, τ is deviatoric stress in megapascals, d is grain size in meters, ϕ is dust volume fraction, and $\dot{\varepsilon}$ is strain rate in s^{-1}. Dislocation creep involves movement of irregularities through the crystal structure causing deformation of individual crystals and has $n = 4$ and $m = 0$ [*Durham et al.*, 1992], although some field studies yield $n = 3$ [*Cuffey and Paterson*, 2010]. GBS involves movement of individual ice grains and has $n = 1.8$ and $m = -1.4$ [*Goldsby and Kohlstedt*, 2001]. Basal slip (sometimes called basal glide) involves movement of dislocations along crystallographic planes and has $n = 2.4$ and $m = 0$ [*Goldsby and Kohlstedt*, 2001]. Diffusion creep [*Raj and Ashby*, 1971] is negligible for the stresses that control viscous flow in our simulations (~0.1–1.0 MPa). Our values for A and Q for each deformation mechanism are from *Goldsby and Kohlstedt* [2001]. The NPLD are not pure ice; for a particular dust volume fraction, the strain rate is $\exp(-2n\phi)$ that of pure ice as in equation (1) [*Durham and Stern*, 2001]. Overall, strain rates for dislocation creep, GBS, and basal slip are, respectively,

$$\dot{\varepsilon}_{\mathrm{dis}} = \frac{3^{2.5}}{2} \times 400,000 e^{-8\phi - \frac{60,000}{RT}} \tau^4 \tag{2}$$

$$\dot{\varepsilon}_{\mathrm{gbs}} = \frac{3^{1.4}}{2} \times 0.0039 e^{-3.6\phi - \frac{49,000}{RT}} \tau^{1.8} d^{-1.4} \tag{3}$$

$$\dot{\varepsilon}_{\mathrm{basal}} = \frac{3^{1.7}}{2} \times 55,000,000 e^{-4.8\phi - \frac{60,000}{RT}} \tau^{2.4} \tag{4}$$

These equations are applicable for temperatures below ~250 K, which is suitable for the Martian poles, and combined to obtain the total strain rate as [*Goldsby and Kohlstedt*, 2001]

$$\dot{\varepsilon}_{\mathrm{total}} = \dot{\varepsilon}_{\mathrm{dis}} + \frac{1}{\frac{1}{\dot{\varepsilon}_{\mathrm{gbs}}} + \frac{1}{\dot{\varepsilon}_{\mathrm{basal}}}} \tag{5}$$

Equations (2)–(4) contain a correction factor of $3^{(n+1)/2}/2$ as the material parameter is typically measured under uniaxial stress in the laboratory [*Cuffey and Paterson*, 2010]. For stresses applicable here, the Glen-Nye flow law (where $n = 3$) and the flow laws of equations (2)–(5) yield strain rates on the same order of magnitude but different by up to ~40%.

Important rheological parameters for our models include ice grain size, dust fraction and distribution, and BU viscosity. Grain size affects GBS, with increasing grain size causing lower flow velocities. If the NPLD are ~2% dust by mass, grain sizes are expected to be ~1 mm for the bulk of the NPLD, though estimates between 1 and 5 mm are possible for lower dust fractions [*Barr and Milkovich*, 2008]. This is consistent with spectral observations of grain size at the surface of the overlying residual cap [*Langevin et al.*, 2005], although as we discuss later this is not necessarily indicative of grain size at depth. We vary grain size between 1 and 5 mm as an input parameter. We consider a uniform dust fraction of 2% as our nominal case according to

the upper limit found by *Picardi et al*. [2005] but vary dust fraction in the NPLD between 0 and 5%, according to limits given by another SHARAD-based study [*Grima et al*., 2009]. BU rheology is not well known, but it is sandier than the PLD [*Herkenhoff et al*., 2007]. We thus consider two end-members: one where the BU is immobile and one where the BU is allowed to flow with the same rheology as the PLD. The true flow velocities likely lie between the two sets of resultant flow velocities for any given model.

We base our inputs for the topography on HiRISE imagery. Analyses of images have revealed that impact craters on the NPLD do not exceed hundreds of meters in diameter [*Banks et al*., 2010; *Landis et al*., 2015]. We model impact craters in 3-D, assuming a 200 m diameter and calculating depths according to the relations of *Garvin et al*. [2000]. We use the findings of *Russell et al*. [2008] to approximate the scarps in 2-D as an 800 m tall quarter-sine wave with a maximum slope of ~70° at their base.

Our models are more sensitive to ice temperature than other parameters. Annual average temperatures for flat NPLD terrain at current Martian obliquity range from ~155 K at the pole to ~170 K at the margins [*Pathare and Paige*, 2005] but are ~200 K for a 70° southwest facing slope at the margin [*Byrne et al*., 2013]. We consider our nominal case to be an annual average temperature of 170 K for craters and 200 K for the maximum slope at the base of a scarp whose annual average temperature varies as a function of slope according to *Byrne et al*. [2013] but vary annual average temperatures over tens of kelvins. Initial modeling suggested a significant thermal gradient with depth for the NPLD [*Larsen and Dahl-Jensen*, 2000] but underestimated the purity of PLD ice and thus the thermal conductivity. Even with this overestimate of the thermal gradient, the ice layer containing a 200 m diameter crater is expected to vary by <1 K with depth, and thus our crater simulations are isothermal (see supporting information for the effects of lateral temperature variability). However, the effect may be important for an 800 m tall scarp. For the scarp modeling, we impose a 30 mW/m^2 basal heat flux [*Clifford*, 1987]. We use the following equations for temperature-dependent heat capacity, c, and thermal conductivity, k, [*Petrenko and Whitworth*, 1999]

$$c = 146.3 + 7.253T \tag{6}$$

$$k = \frac{651}{T} \tag{7}$$

These are estimates for pure ice. PLDs may have enough dust to alter c and k, but we will see that effects from heat flux, thermal conductivity, and heat capacity are very small compared to the effect of the annual average surface temperature. Diurnal and seasonal cycles cause the near-surface ice temperature to oscillate about the annual average. While the amplitude of this thermal wave is large (~40 K), it only penetrates ~10 m into the ice [*Byrne et al*., 2013], and these scarps are hundreds of meters in scale. Since the thermal wave affects the scarp face, we are likely not capturing complexities in seasonally varying flow, but because of the shallow wave penetration, only a small percentage of ice is affected.

We use a domain size in our model runs of 2 km in all dimensions for a 200 m wide crater and 5 km long and 2 km high for a 2-D 800 m tall scarp. Our results do not significantly change with doubling the domain size. We mesh these domains with nodes every 25 m, and our results do not significantly change with doubling the node density. We set a boundary condition such that the top surface of our models is a free surface with temperature equal to the annual average appropriate for the slope at each point and, for cases of scarps atop an immobile BU, no sliding at the base. For cases atop a mobile BU, the bedrock 1 km under the BU is immobile.

3. Results and Discussion

The impact crater shown in Figure 1 is a 200 m diameter crater with temperature 170 K, dust fraction 2%, and grain size 1 mm. We additionally show flow velocities in a cross section of ice through the crater's center. *Pathare et al*. [2005] modeled larger craters in the SPLD due to the lack of observed craters in the NPLD at the time, but our flow velocities are consistent with theirs when one takes into account the difference in parameters between the two studies, most importantly crater size (see supporting information). Flow velocities of impact craters are maximized at the center of the structure, causing the floor to raise and the walls to shallow. However, these velocities do not exceed μm/yr for any reasonable combination of parameters. Even in the impossible scenario that craters are as old as the maximum age of the whole NPLD (~5 Myr) estimated by thermal modeling while considering orbital variations [*Levrard et al*., 2007], an NPLD crater at 170 K would

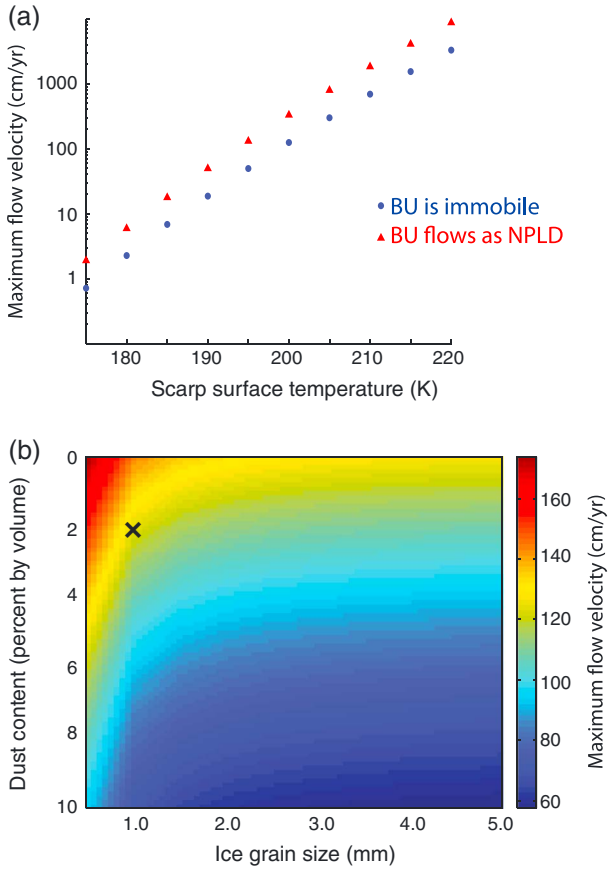

Figure 3. Sensitivity of scarp results to parameters. (a) Maximum flow velocity as a function of the annual average surface temperature on the steepest slope of the scarp. We show cases where the underlying BU underlying is immobile (blue) and has the same rheology as the NPLD (red). (b) Maximum flow velocity as a function of ice grain size and dust content in the NPLD for an immobile BU; our nominal case (2% dust volume, grain size 1 mm) is marked with a cross.

not shallow by more than a few meters over its lifetime. The actual crater retention age of the NPLD surface is 2–3 orders of magnitude less than the 5 Myr constraint [*Banks et al.*, 2010; *Landis et al.*, 2015], so flow velocities are far too small for viscous relaxation to appreciably modify the NPLD craters presently observed. This is in contrast to the SPLD, where larger and older craters likely experience significant viscous relaxation [*Pathare et al.*, 2005]. Our NPLD result lends credibility to model ages derived from observed size-frequency distributions, which imply that the NPLD surface is only approximately kiloyears old [*Landis et al.*, 2015]. This young surface cannot be due to crater removal from viscous relaxation. Instead, ice accumulation (resulting in crater infill) is likely responsible for the young NPLD surface model age.

Steep scarps at NPLD margins with dust fraction of 2%, grain size of 1 mm, and immobile BU have stresses, flow velocities, and temperatures as shown in Figure 2. Maximum flow velocities are near the lower face of the scarp and are of order 1 m/yr for an annual average surface temperature of 200 K, and higher if the BU can flow as pure ice. Because the BU is much sandier than the PLD [*Byrne and Murray*, 2002; *Fishbaugh and Head*, 2005], we expect that models with an immobile BU represent the flow more accurately. Flow is primarily outward at the scarp base and primarily downward at the scarp top, meaning that the scarp slope is shallowing over time. Our flow velocities are higher than those found by *Hvidberg* [2003], which calculated velocities on the order of cm/yr for troughs and scarps, but that study considered scarps with shallower slopes (~15°), so our faster modeled flow of newly discovered steeper scarps is not inconsistent.

Figure 3 shows sensitivity of the flow to various input parameters. As expected, flow velocity is most sensitive to ice temperature. For a given set of other parameters, an increase in annual average surface temperature of 10 K corresponds to an increase in the maximum flow velocity of a topographic feature by approximately an order of magnitude (Figure 3a). Because we model a relatively low basal heat flux (30 mW/m^2), the thermal gradient away from the surface is also low and the temperature of the ice that experiences flow is very close to the annual average surface temperature. Another study that analyzed lithospheric deflection from NPLD and BU loading concluded a lower heat flux of ~8 mW/m^2 [*Phillips et al.*, 2008]. Therefore, while the heat flux has high uncertainty, it is not a large factor in controlling flow; we performed model runs with an unrealistically high basal flux of 60 mW/m^2 and found that the resulting temperatures were at most ~1.5 K greater compared to the runs with 30 mW/m^2, and even these temperature increases occurred where flow velocities were minimal far from the scarp face.

Unknown parameters with potential for greater control of flow are dust content and ice grain size (Figure 3b). Here we have assumed a uniform grain size. For models with a grain size of 1 mm (Figure 2), we find that

dislocation creep accounts for ~85% of the strain rate and GBS accounts for the remaining ~15%. Dislocation creep is independent of grain size (equation (2)), and strain rate due to GBS decreases with increasing grain size (equation (3)), so the flow velocity due to dislocation creep can be interpreted as a minimum. Although the exact grain size distribution is unknown in the PLDs, it generally increases with depth in terrestrial ice sheets [e.g., *Thorsteinsson et al*., 1997; *Durand et al*., 2006], and thus we can conclude that this uncertainty is not changing the order of magnitude of our results. Even if sharp transitions in grain size exist as in some terrestrial ice sheets [e.g., *Duval and Lorius*, 1980], large effects are unexpected if grain size is >0.1 mm (Figure 3b). Even for cases where dust content and grain size values are likely too high, our results still show flow on the order of tens of cm/yr.

Our results imply that observed steep scarps would have taken approximately kiloyears to flow into their present shape if they began as a nearly vertical cliff and are not currently in a steady state. However, this timescale is only valid if there are no other factors that modify the topography. An alternate possibility is that the scarps are older and have a steady state shape, where other effects compete with viscous flow by steepening the slope. Observed avalanches [*Russell et al*., 2008] and block falls [*Russell et al*., 2012] and their possible effects on the thermal properties and mass wasting of the PLD should be considered.

A key observation from HiRISE imagery is that mass wasting of meter-scale ice blocks is common, as evidenced by basal debris [*Russell et al*., 2012]. However, the avalanches are composed of dust and CO_2 frost and are thus not directly responsible for block falls [*Russell et al*., 2008]. Instead, avalanches may have an important indirect effect on the thermal properties of the scarps by scouring away their dust cover that accumulates as a sublimation lag. Dust deposits are an important mechanism in shielding ice from ablation on Mars [e.g., *Toon et al*., 1980] and elsewhere [*Schorghofer*, 2008; *Spencer and Denk*, 2010; *Hayne and Aharonson*, 2015]. Without a dust cover, the equatorward facing scarps experience large thermal stresses that easily exceed the tensile stress of ice, causing fractures [*Byrne et al*., 2013]. These fractures can lead to mass wasting that steepens the slope to counteract the shallowing that occurs from viscous flow. We estimate based on integrating our results forward in time 1 year that such mass wasting would (when combined with ablation) need to transport hundreds of m^3/yr for each meter along the scarp to maintain steady state. In the absence of flow, enough blockfalls and ablation would be occurring to cause a scarp retreat rate of tens of cm/yr. One note of importance in thermal modeling is that the Martian poles experience high-amplitude changes in insolation, mostly as a result of a quasiperiodic obliquity cycle with period ~120 kyr [*Laskar et al*., 2002]. If the scarps had a comparable age to this period, their steady state topography would likely change over time, as rates of viscous flow and thermally induced block fall would both change.

4. Conclusions

Present-day impact craters on the NPLD experience insufficient stresses and temperatures for viscous relaxation to be an important modification mechanism in shaping their topography. Studies that analyze NPLD crater morphology or derive model ages for NPLD surfaces using impact crater size-frequency distributions do not need to consider viscous relaxation of craters as an important effect. In contrast, scarps at the margins of the NPLD are comparatively high relief, steep, and warm. Modeling that considers scarp geometry, surface temperature, basal heat flux, ice grain size, and dust content shows that viscous flow must be an important mechanism acting upon the scarps over the lifetime of the NPLD, with flow rates on the order of tens to hundreds of cm/yr. If there were no other processes shaping topography, scarps would flow into their presently observed shape from an initial vertical cliff in kiloyears and continue flowing. However, given observations of dust/frost avalanches, ice block falls, and thermal modeling that shows thermal stresses on the scarps exceed the tensile strength of the PLD, it is more likely that scouring of dust off the scarps leads to thermal stress-induced mass wasting which steepens the scarps in a competing effect to that of shallowing viscous flow.

A tantalizing prospect is the possibility of observing active viscous flow. Our favored model (Figure 2) yields a maximum flow velocity of ~1 m/yr. Even if viscous flow and block falls provide competing effects as described above, the discrete nature of block falls means that a steady state is not achieved perfectly, and the continuous viscous flow may still be observable. Additionally, flow would decrease the elevation of the scarp top, which would not be countered by block falls. SHARAD analysis is implausible for steep scarps due to complications in observing the subsurface close to even moderately sloping features [*Christian et al*., 2013]. However, HiRISE images have resolutions of ~30 cm/pixel, and HiRISE observations of scarps began in 2008

[*Russell et al*., 2008]. Our modeling predicts that scarps flow several pixels in an image over the lifetime of the instrument, and therefore analyses of future digital elevation models of the same scarp may be able to observe ice flow. Such observations would allow us to constrain parameters with our models; lower flow rates than predicted could indicate higher dust content or colder ice than expected.

Acknowledgments
This work was funded by grant NNX13AG72G of the Mars Fundamental Research Program. HiRISE imagery referenced in this paper can be found on the instrument's public website, https://hirise.lpl.arizona.edu. We thank two anonymous reviewers for their constructive remarks.

References

Arthern, R. J., D. P. Winebrenner, and E. D. Waddington (2000), Densification of water ice deposits on the residual north polar cap of Mars, *Icarus*, *144*, 367–381, doi:10.1006/icar.1999.6308.

Banks, E. M., S. Byrne, K. Galla, A. S. McEwen, V. J. Bray, C. M. Dundas, K. E. Fishbaugh, K. E. Herkenhoff, and B. C. Murray (2010), Crater population and resurfacing of the Martian north polar layered deposits, *J. Geophys. Res.*, *115*, E08006, doi:10.1029/2009JE003523.

Barr, A. C., and S. M. Milkovich (2008), Ice grain size and the rheology of the Martian polar deposits, *Icarus*, *194*, 513–518, doi:10.1016/j.icarus.2007.11.018.

Bland, M. T., K. N. Singer, W. B. McKinnon, and P. M. Schenk (2012), Enceladus' extreme heat flux as revealed by its relaxed craters, *Geophys. Res. Lett.*, *39*, L17204, doi:10.1029/2012GL052736.

Byrne, S. (2009), The polar deposits of Mars, *Annu. Rev. Earth Planet. Sci.*, *37*, 535–560, doi:10.1146/annurev.earth.031208.100101.

Byrne, S., and B. C. Murray (2002), North polar stratigraphy and the paleo-erg of Mars, *J. Geophys. Res.*, *107*, E65044, doi:10.1029/2001JE001615.

Byrne, S., P. S. Russell, A. Pathare, P. Becerra, J. Molaro, S. Mattson, and M. T. Mellon (2013), Fracturing the icy polar cliffs of Mars, Lunar Planet. Sci. Conf., 44th, 1659.

Christian, S., J. W. Holt, S. Byrne, and K. E. Fishbaugh (2013), Integrating radar stratigraphy with high resolution visible stratigraphy of the north polar layered deposits Mars, *Icarus*, *226*, 1241–1251, doi:10.1016/j.icarus.2013.07.003.

Clifford, S. M. (1987), Polar basal melting on Mars, *J. Geophys. Res.*, *92*, 9135–9152, doi:10.1029/JB092iB09p09135.

Cuffey, K. M., and W. S. B. Paterson (2010), *The Physics of Glaciers*, 4th ed., Butterworth-Heinemann publications, Burlington, MA, USA.

Daubar, I. J., A. S. McEwen, S. Byrne, M. R. Kennedy, and B. Ivanov (2013), The current Martian cratering rate, *Icarus*, *225*, 506–516, doi:10.1016/j.icarus.2013.04.009.

Dombard, A. J., and W. B. McKinnon (2000), Long-term retention of impact crater topography on Ganymede, *Geophys. Res. Lett.*, *27*, 3633–3666, doi:10.1029/2000GL011695.

Durand, G., et al. (2006), *J. Geophys. Res.*, *111*, F01015, doi:10.1029/2005JF000320.

Durham, W. B., and L. A. Stern (2001), Rheological properties of water ice—Applications to satellites of the outer planets, *Annu. Rev. Earth Planet. Sci.*, *29*, 295–330, doi:10.1146/annurev.earth.29.1.295.

Durham, W. B., S. H. Kirby, and L. A. Stern (1992), Effects of dispersed particulates on the rheology of water ice at planetary conditions, *J. Geophys. Res.*, *97*, 20,883–20,897, doi:10.1029/92JE02326.

Duval, P., and C. Lorius (1980), Crystal size and climatic record down to the last ice age from Antarctic ice, *Earth Planet. Sci. Lett.*, *48*, 59–64, doi:10.1016/0012-821X(80)90170-3.

Fishbaugh, K. E., and J. W. Head (2005), Origin and characteristics of the Mars north polar basal unit and implications for polar geologic history, *Icarus*, *174*, 444–474, doi:10.1016/j.icarus.2004.06.021.

Gagliardini, O., et al. (2013), Capabilities and performance of Elmer/Ice, a new-generation ice sheet model, *Geosci. Model Dev.*, *6*, 1299–1318, doi:10.5194/gmd-6-1299-2013.

Garvin, J. B., S. E. H. Sakimoto, J. J. Frawley, and C. Schnetzler (2000), North polar region craterforms on Mars: Geometric characteristics from the Mars Orbiter Laser Altimeter, *Icarus*, *144*, 329–352, doi:10.1006/icar.1999.6298.

Glen, J. W. (1955), The creep of polycrystalline ice, *Proc. R. Soc. London, Ser. A*, *228*, 519–538.

Goldsby, D. L., and D. L. Kohlstedt (2001), Superplastic deformation of ice: Experimental observations, *J. Geophys. Res.*, *106*, 11,017–11,030, doi:10.1029/2000JB900336.

Greve, R. (2000), Waxing and waning of the perennial north polar H_2O ice cap of Mars over obliquity cycles, *Icarus*, *144*, 419–431, doi:10.1006/icar.1999.6291.

Grima, C., W. Kofman, J. Mouginot, R. J. Phillips, A. Herique, D. Biccari, R. Seu, and M. Cutigni (2009), North polar deposits of Mars: Extreme purity of water ice, *Geophys. Res. Lett.*, *36*, L03203, doi:10.1029/2008GL036326.

Hayne, P. O., and O. Aharonson (2015), Thermal stability of ice on Ceres with rough topography, *J. Geophys. Res. Planets*, *120*, 1567–1584, doi:10.1002/2015JE004887.

Herkenhoff, K., S. Byrne, P. Russell, K. Fishbaugh, and A. McEwen (2007), Meter-scale morphology of the north polar region of Mars, *Science*, *317*, 1711–1715, doi:10.1126/science.1143544.

Howard, A. D. (1978), Origin of the stepped topography of the Martian poles, *Icarus*, *34*, 581–599, doi:10.1016/0019-1035(78)90047-7.

Hvidberg, C. (2003), Relationship between topography and flow in the north polar cap on Mars, *Ann. Glaciol.*, *37*, 363–369, doi:10.3189/172756403781815906.

Ivanov, A. B., and D. O. Muhleman (2000), The role of sublimation for the formation of the northern ice cap: Results from the Mars orbiter laser altimeter, *Icarus*, *144*, 436–448, doi:10.1006/icar.1999.6304.

Karlsson, N. B., J. W. Holt, and R. C. A. Hindmarsh (2011), Testing for flow in the north polar layered deposits of Mars using radar stratigraphy and a simply 3D ice-flow model, *Geophys. Res. Lett.*, *38*, L24202, doi:10.1029/2011GL049630.

Koutnik, M., S. Byrne, and B. Murray (2002), South polar layered deposits of Mars: The cratering record, *J. Geophys. Res. 107*(E11), 5100, doi:10.1029/2001JE001805.

Landis, M. E., S. Byrne, I. J. Daubar, K. E. Herkenhoff, and C. M. Dundas (2015), Reinterpreting the impact craters of the north polar layered deposits, Lunar Planet. Sci. Conf. 46th, 1294.

Langevin, Y., F. Poulet, J.-P. Bibring, B. Schmitt, S. Doute, and B. Gondet (2005), Summer evolution of the north polar cap of Mars as observed by OMEGA/Mars Express, *Science*, *307*, 1581–1584, doi:10.1126/science.1109438.

Larsen, J., and D. Dahl-Jensen (2000), Interior temperatures of the northern polar cap on Mars, *Icarus*, *144*, 456–462, doi:10.1006/icar.1999.6296.

Laskar, J., B. Levrard, and J. F. Mustard (2002), Orbital forcing of the Martian polar layered deposits, *Nature*, *419*, 375–377, doi:10.1038/nature01066.

Levrard, B., F. Forget, F. Montmessin, and J. Laskar (2007), Recent formation and evolution of northern Martian polar layered deposits as inferred from a global climate model, *J. Geophys. Res.*, *112*, E06012, doi:10.1029/2006JE002772.

McEwen, A. S., et al. (2007), Mars Reconnaissance Orbiter's High Resolution Imaging Science Experiment (HiRISE), *J. Geophys. Res.*, *112*, E05S02, doi:10.1029/2005JE002605.
Mellon, M. T. (1996), Limits on the CO_2 content of the Martian polar layered deposits, *Icarus*, *124*, 268–279, doi:10.1006/icar.1996.0203.
Melosh, H. J. (2011), *Planetary Surface Processes*, Cambridge Univ. Press, Cambridge, U. K.
Milliken, R. E., J. F. Mustard, and D. L. Goldsby (2003), Viscous flow features on the surface of Mars: Observations from high-resolution Mars Orbiter Camera (MOC) images, *J. Geophys. Res.*, *108*(E6), 5057, doi:10.1029/2002JE002005.
Miyamoto, H., G. Mitri, A. P. Showman, and J. M. Dohm (2005), Putative ice flows on Europa: Geometric patterns and relation to topography collectively constrain material properties and effusion rates, *Icarus*, *177*, 413–424, doi:10.1016/j.icarus.2005.03.014.
Murray, B. C., L. A. Soderblom, J. A. Cutts, R. P. Sharp, D. J. Milton, and R. B. Leighton (1972), Geological framework of the south polar region of Mars, *Icarus*, *17*, 328–345, doi:10.1016/0019-1035(72)90004-8.
Nimmo, F. (2005), Tectonic consequences of Martian dichotomy modification by lower-crustal flow and erosion, *Geology*, *33*, 533–536, doi:10.1130/G21342.1.
Nye, J. F. (2000), A flow model for the polar caps of Mars, *J. Glaciol.*, *46*, 438–444.
Nye, J. F., W. B. Durham, P. M. Schenk, and J. M. Moore (2000), The instability of a south polar cap on Mars composed of carbon dioxide, *Icarus*, *144*, 449–455, doi:10.1006/icar.1999.6306.
Pathare, A. V., and D. A. Paige (2005), The effects of Martian orbital variations upon the sublimation and relaxation of north polar troughs and scarps, *Icarus*, *174*, 419–443, doi:10.1016/j.icarus.2004.10.030.
Pathare, A. V., D. A. Paige, and E. Turtle (2005), Viscous relaxation of craters within the Martian south polar layered deposits, *Icarus*, *174*, 396–418, doi:10.1016/j.icarus.2004.10.031.
Petrenko, V. F., and R. W. Whitworth (1999), *Physics of Ice*, Oxford Univ. Press, Oxford, U. K.
Phillips, R. J., et al. (2008), Mars north polar deposits: Stratigraphy, age, and geodynamical response, *Science*, *320*, 1182–1185, doi:10.1126/science.1157546.
Phillips, R. J., et al. (2011), Massive CO_2 ice deposits sequestered in the south polar layered deposits of Mars, *Science*, *332*, 838–841, doi:10.1126/science/1203091.
Picardi, G., et al. (2005), Radar soundings of the subsurface of Mars, *Science*, *310*, 1925–1928, doi:10.1126/science.1122165.
Plaut, J. J., et al. (2007), Subsurface radar sounding of the south polar layered deposits of Mars, *Science*, *316*, 92–96, doi:10.1126/science.1139672.
Raj, R., and M. F. Ashby (1971), On grain boundary sliding and diffusional creep, *Metall. Trans.*, *2*, 1113–1127.
Russell, P., et al. (2008), Seasonally active frost-dust avalanches on a north polar scarp of Mars captured by HiRISE, *Geophys. Res. Lett.*, *35*, L23204, doi:10.1029/2008GL035790.
Russell, P., S. Byrne, A. Pathare, and K. E. Herkenhoff (2012), Active erosion and evolution of Mars north polar scarps, Lunar Planet. Sci. Conf., 43rd, 2747.
Schorghofer, N. (2008), The lifetime of ice on main belt asteroids, *Astrophys. J.*, *682*, 697–705, doi:10.1086/588633.
Smith, I. B., J. W. Holt, A. Spiga, A. D. Howard, and G. Parker (2013), The spiral troughs of Mars as cyclic steps, *J. Geophys. Res. Planets*, *118*, 1835–1857, doi:10.1002/jgre.20142.
Spencer, J. R., and T. Denk (2010), Formation of Iapetus' extreme albedo dichotomy by exogenically triggered thermal ice migration, *Science*, *22*(327), 432–435, doi:10.1126/science.1177132.
Squyres, S. W. (1978), Martian fretted terrain: Flow of erosional debris, *Icarus*, *34*, 600–613, doi:10.1016/0019-1035(78)90048-9.
Thomas, P. J., and G. Schubert (1988), Power law rheology of ice and the relaxation style and retention of craters on Ganymede, *J. Geophys. Res.*, *93*, 13,755–13,762, doi:10.1029/JB093iB11p13755.
Thorsteinsson, T., T. J. Kipfstul, and H. Miller (1997), Textures and fabrics in the GRIP ice core, *J. Geophys. Res.*, *102*, 26,583–26,600, doi:10.1029/97JC00161.
Toon, O. B., J. B. Pollack, W. Ward, J. A. Burns, and K. Bilski (1980), The astronomical theory of climate changes on Mars, *Icarus*, *44*, 552–607.
Wieczorek, M. A. (2008), Constraints on the composition of the Martian south polar cap from gravity and topography, *Icarus*, *196*, 506–517, doi:10.1016/j.icarus.2007.10.026.
Winebrenner, D. P., M. R. Koutnik, E. D. Waddington, A. V. Pathare, B. C. Murray, S. Byrne, and J. Bamber (2008), Evidence for ice flow prior to trough formation in the Martian north polar layered deposits, *Icarus*, *195*, 90–105, doi:10.1016/j.icarus.2007.11.030.
Zuber, M. T., et al. (1998), Observations of the north polar region of Mars from the Mars Orbiter Laser Altimeter, *Science*, *282*, 2053–2060, doi:10.1126/science.282.5396.2053.
Zuber, M. T., R. J. Phillips, J. C. Andrews-Hanna, S. W. Asmar, A. S. Konopliv, F. G. Lemoine, J. J. Plaut, D. E. Smith, and S. E. Smrekar (2007), Density of Mars' south polar layered deposits, *Science*, *317*, 1718–1719, doi:10.1126/science.1146995.
Zwinger, T., R. Greve, O. Gagliardini, T. Shiraiwa, and M. Lyly (2007), A full Stokes-flow thermo-mechanical for firn and ice applied to the Gorshkov crater glacier, Kamchatka, *Ann. Glaciol.*, *45*, 29–37, doi:10.3189/172756407782282543.